CHAPTER 8

ANALYSIS OF AVERAGE SQUARED DIFFERENCE SURFACES

In Chapters 5, 6, and 7, the Spectral Fit algorithm was used to estimate both scatterer size and total attenuation from the backscattered waveforms by minimizing the average squared difference (*ASD*) given by Equation (5.3). However, the *ASD* surface over which the minimization is to be performed has not yet been analyzed. If the surface has a local minimum, then the global minimum could not be found by the simple minimization routine that was utilized in the previous chapters and a more complicated implementation of the algorithm would be required. In addition, the properties of the *ASD* surface might provide insight into the puzzling dependence of the precision on the initial ka_{eff} values for different sources discussed in Section 7.3. Hence, in this chapter, an analysis is performed of the *ASD* surface. The analysis considers the impact scatterer size, half-space attenuation, spectral variance resulting from random scatterer spacing, frequency range, Δka_{eff} range, and initial frequency have on the shape of the *ASD* surface. The analysis is done using the simulated backscattered waveforms from the earlier chapters as well as through mathematical derivations. The changes of the shape of the *ASD* surface were then related to the precision of the Spectral Fit algorithm.

8.1 Properties of *ASD* Surfaces from Simulated Waveforms

Initially, the features of the *ASD* surface were investigated using some of the simulated data generated for the half-spaces discussed in the previous chapters. The investigation was done by observing qualitative changes in the overall structure of the surface with changes in the properties of the half-space. An example *ASD* surface for a half-space with an attenuation of 0.3 dB/cm/MHz containing Gaussian scatterers with effective radii of 25 μm at a density of 35/mm^3 is shown in Figure 8.1. This surface was generated by solving for *ASD* using Equation (5.3) for different input values of scatterer size and total attenuation. In the figure, the colors correspond

to the 1/*ASD* values. Normally, the Spectral Fit algorithm would yield the scatterer size and total attenuation corresponding to the minimum *ASD* value. When generating this surface, P_{scat} was found by averaging in the normal spectral domain the first 25 waveforms (1st set of 40 sets) of the 1000 waveforms that had been generated for this half-space using a source with filtering characteristics given by Equation (7.5). The waveforms had been windowed in the time domain by a hamming window with a length of 2.5 mm and the frequency range selected, over which the mean value in Equation (5.3) was found, was given by Equation (7.2). Although the width of the trough (i.e., light red portion in image) was different for the different sets, as can be observed in Appendix F, the surfaces corresponding to the other sets were not qualitatively different from the one shown. However, the width of the trough did not correlate with the accuracy of the final estimate (i.e., see 13th and 14th sets in Appendix F).

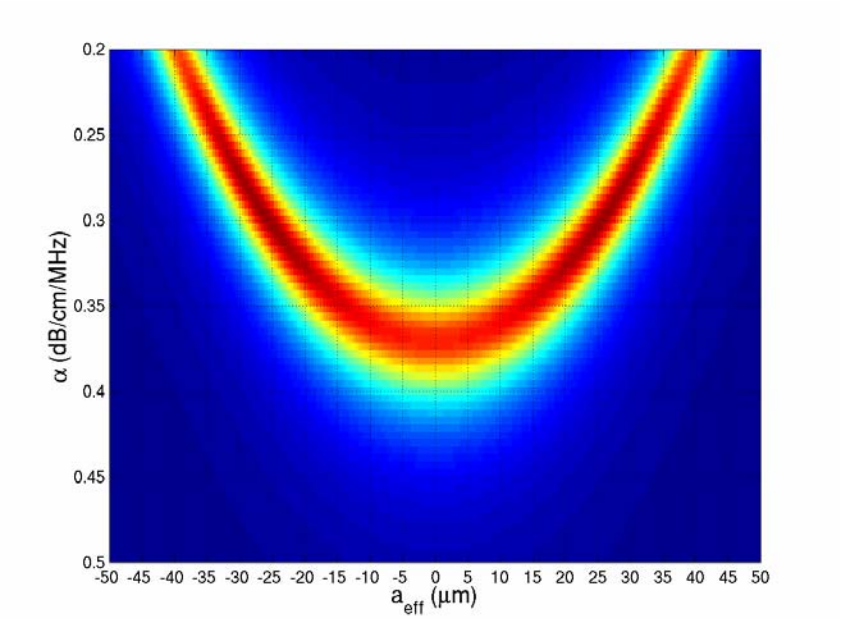

Figure 8.1: Example *ASD* surface for a half-space with an attenuation of 0.3 dB/cm/MHz containing 25 μm scatterers generated from 25 waveforms windowed with a 2.5 mm hamming window from a source whose filtering function $H(f)$ was given by Equation (7.5). Dark red corresponds to a small *ASD* value and dark blue corresponds to a large *ASD* value. The minimum for this surface (dark red) occurs at a scatterer size of 26.6 μm.

The *ASD* surface varies smoothly throughout the entire region with only one minimum. Hence, our simple minimization routine employed in Matlab was appropriate. Also, there is a range of a_{eff} and α values for which the *ASD* values are relatively small as is seen by the parabolic light red region of the image. It was observed in Appendix F that the location of the minimum is always found along this *parabolic trough*, even when it does not occur at the correct

value for scatterer size and total attenuation. The parabolic trough is symmetric about a_{eff} = 0 μm because a_{eff} is squared in the evaluation of the Gaussian form factor. Of course, a negative value for scatterer size is not physical and hence would only be a mathematical peculiarity.

After establishing the basic shape of the ASD surface, the influence of the different half-space parameters on this basic shape was investigated. Hence, an *ASD* surface, shown in Figure 8.2, was generated corresponding to the first 25 waveforms (1st set of 40 sets) for a half-space with a half-space attenuation of 0.5 dB/cm/MHz that still contained Gaussian scatterers with effective radii of 25 μm at a density of 35/mm^3. The frequency range was once again selected by Equation (7.2) and a hamming window with a length of 2.5 mm was still used to gate the time domain signals. Now the parabolic trough intersects the a_{eff} = 0 μm axis at ~0.55 dB/cm/MHz. However, the same change in scatterer size results in the same change in attenuation along the parabolic trough. Hence, the attenuation appears to shift the surface to higher values of attenuation without affecting the overall shape of the surface.

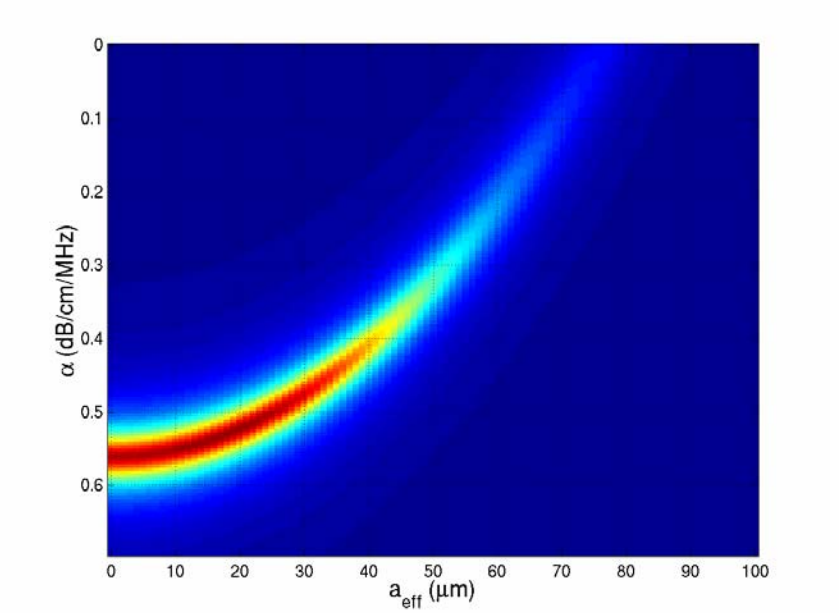

Figure 8.2: Example *ASD* surface for a half-space with an attenuation of 0.5 dB/cm/MHz containing 25 μm scatterers generated from 25 waveforms windowed with a 2.5 mm hamming window from a source whose filtering function $H(f)$ was given by Equation (7.5). Dark red corresponds to a small *ASD* value and dark blue corresponds to a large *ASD* value. The minimum for this surface (dark red) occurs at a scatterer size of 18.0 μm.

After assessing the impact of attenuation on the *ASD* surface, the effect of different scatterer sizes was evaluated. Hence, *ASD* surfaces, shown in Figures 8.3 and 8.4, were

generated corresponding to two half-spaces containing scatterers with a_{eff} of 5 μm and 45 μm, respectively. The attenuation of the half-spaces was maintained at 0.3 dB/cm/MHz while the source and windowing parameters were the same as the previous two surface plots. Once again, the different scatterer sizes appear to primarily shift the *ASD* surfaces along the α axis with the smaller scatterer sizes shifting the surface to smaller α values and the larger scatterer size shifting the surface to large α values. However, the area colored light red in the figures relative to the true scatterer size appears to be much smaller as the scatterer size is increased. Hence, the minimum is more pronounced for the larger sized scatterers.

Once the impact of attenuation and scatterer size on the *ASD* surface was determined, the influence of window length was investigated because the earlier results indicated that the precision of the estimates should be improved by increasing the length of the window used to gate the time domain signals. Figure 8.5 shows the *ASD* surface for the same waveforms used to generate the *ASD* surface in Figure 8.2, only with a hamming window of length of 8 mm instead of 2.5 mm. The *ASD* surface in Figure 8.5 is indistinguishable from the *ASD* surface in Figure 8.2. Hence, although the larger window lengths improve the precision of the Spectral Fit algorithm, the improvement does not appear to result from any changes to the overall structure of the *ASD* surface. However, it may be that the changes are not visible in this simple qualitative comparison of the surfaces.

After exploring the impact of window length, the effect of different frequency ranges on the *ASD* surface, while maintaining the same Δka_{eff} range, was investigated. Figure 8.6 shows the *ASD* surface corresponding to the first 25 waveforms (1st set of 40 sets) of the 1000 waveforms that had been generated for a half-space with an attenuation of 0 dB/cm/MHz containing Gaussian scatterers with effective radii of 25 μm. The source used to generate the waveforms had filtering characteristics given by Equation (7.4), and the waveforms had been windowed in the time domain by a hamming window with a length of 3 mm. Frequencies corresponding to ka_{eff} values of 0.5 to 1.5 were used to find the *ASD*. Likewise, Figure 8.7 shows the *ASD* surface corresponding to the first 25 waveforms (1st set of 40 sets) of the 1000 waveforms that had been generated for a half-space with an attenuation of 0 dB/cm/MHz containing scatterers with effective radii of 50 μm using the same source and window length. The frequency range for Figure 8.7 was given by the frequencies corresponding to ka_{eff} values of 1 to 2 (same initial frequency and Δka_{eff} range but different frequency range).

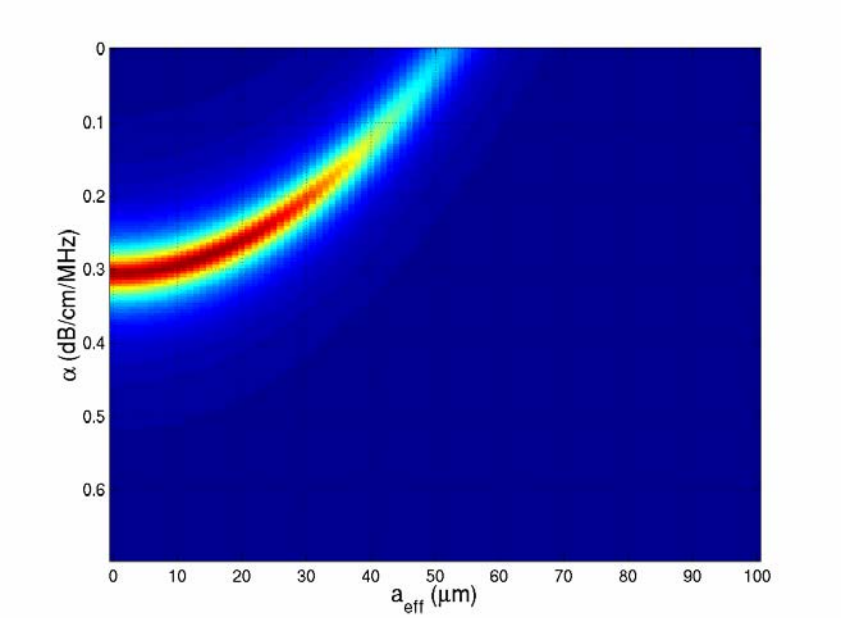

Figure 8.3: Example *ASD* surface for a half-space with an attenuation of 0.3 dB/cm/MHz containing 5 μm scatterers generated from 25 waveforms windowed with a 2.5 mm hamming window from a source whose filtering function $H(f)$ was given by Equation (7.5). Dark red corresponds to a small *ASD* value and dark blue corresponds to a large *ASD* value. The minimum for this surface (dark red) occurs at a scatterer size of 13.2 μm.

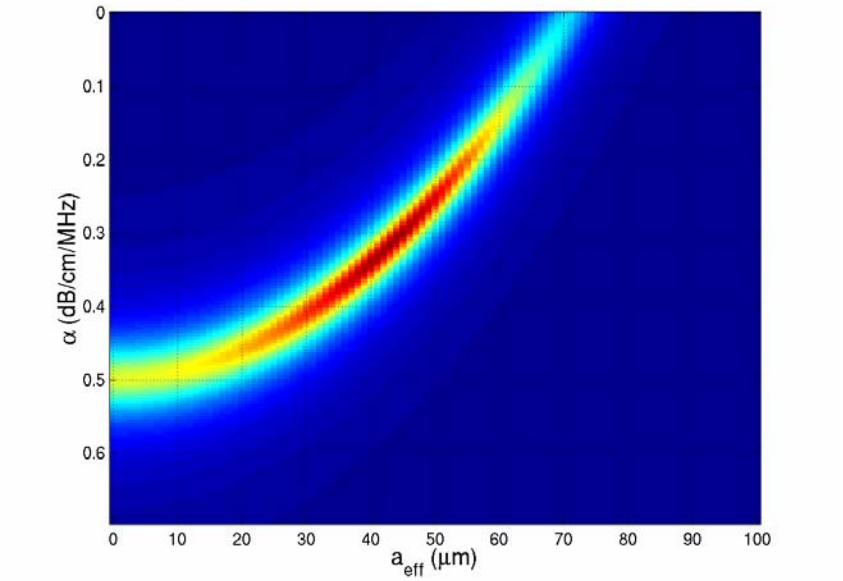

Figure 8.4: Example *ASD* surface for a half-space with an attenuation of 0.3 dB/cm/MHz containing 45 μm scatterers generated from 25 waveforms windowed with a 2.5 mm hamming window from a source whose filtering function $H(f)$ was given by Equation (7.5). Dark red corresponds to a small *ASD* value and dark blue corresponds to a large *ASD* value. The minimum for this surface (dark red) occurs at a scatterer size of 43.0 μm.

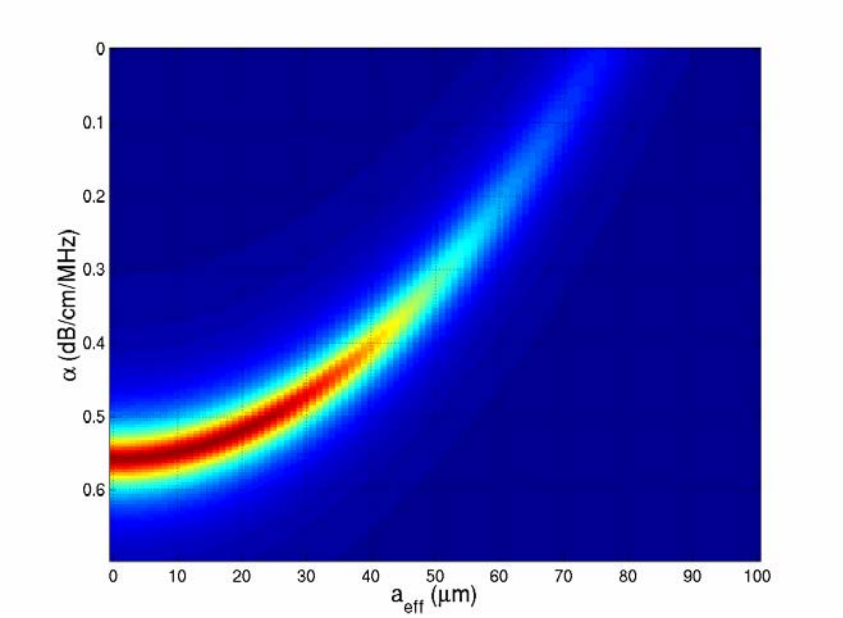

Figure 8.5: Example *ASD* surface for a half-space with an attenuation of 0.5 dB/cm/MHz containing 25 μm scatterers generated from 25 waveforms windowed with a 8 mm hamming window from a source whose filtering function $H(f)$ was given by Equation (7.5). Dark red corresponds to a small *ASD* value and dark blue corresponds to a large *ASD* value. The minimum for this surface (dark red) occurs at a scatterer size of 15.8 μm.

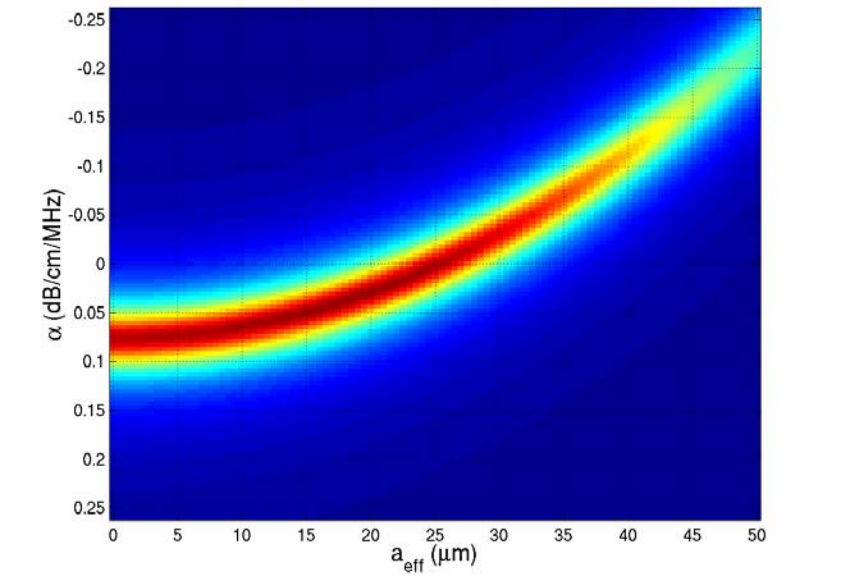

Figure 8.6: Example *ASD* surface for a half-space with an attenuation of 0 dB/cm/MHz containing 25 μm scatterers generated from 25 waveforms windowed with a 3 mm hamming window from a source whose filtering function $H(f)$ was given by Equation (7.4) using frequencies in the ka_{eff} range of 0.5 to 1.5. Dark red corresponds to a small *ASD* value and dark blue corresponds to a large *ASD* value. The minimum for this surface (dark red) occurs at a scatterer size of 18.4 μm.

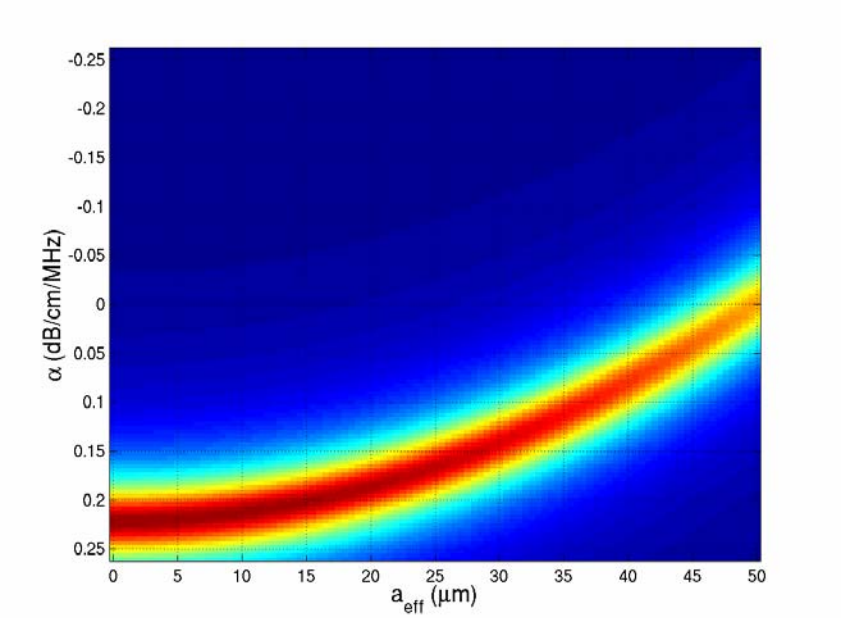

Figure 8.7: Example *ASD* surface for a half-space with an attenuation of 0 dB/cm/MHz containing 50 μm scatterers generated from 25 waveforms windowed with a 3 mm hamming window from a source whose filtering function $H(f)$ was given by Equation (7.4) using frequencies in the ka_{eff} range of 1 to 2. Dark red corresponds to a small *ASD* value and dark blue corresponds to a large *ASD* value. The minimum for this surface (dark red) occurs at a scatterer size of .0196 nm.

By comparing Figures 8.6 and 8.7, one can observe that the *ASD* surface has once again been shifted to larger α values for the larger scatterer size. Furthermore, the parabola describing the parabolic trough has been broadened when a smaller frequency range was used (Figure 8.7). Hence, a change in a_{eff} produces a smaller change in α along the trough in Figure 8.7 as compared to Figure 8.6. Also, the minimum is more pronounced for the smaller sized scatterers when the larger frequency range was selected. When compared to the results in Figure 8.4, this suggests that the more pronounced minimum observed earlier for the larger scatterer sizes was probably due to the increased Δka_{eff} range just as the more pronounced minimum in this case is probably due to the increased frequency range.

Another effect observed in Chapter 7 was the dependence of the precision on the initial frequency used in the minimization routine (i.e., Section 7.3). This dependence was also shown to be related to the peak frequency of the ideal backscattered spectrum. Hence, the next goal was to determine if the dependence on the initial frequency and the corresponding relationship to the peak of the backscattered spectrum could be observed by analyzing the appropriate *ASD* surfaces.

First, only the dependence on the initial frequency was considered by using the same waveforms associated with the *ASD* surface shown in Figure 8.6 in order to generate Figure 8.8. This time, however, the frequency range used in the *ASD* calculation was given by the frequencies corresponding to ka_{eff} values of 1.5 to 2.5 instead of ka_{eff} values of 0.5 to 1.5. All other half-space and processing parameters were the same. Hence, the only difference between the two surfaces would be the initial frequency selected for the calculation. An initial ka_{eff} value of 1.5 corresponds to an initial frequency after the deviation peak (good precision for this source) while an initial ka_{eff} value of 0.5 corresponds to an initial frequency three-quarters of the way up the deviation peak (poor precision for this source), as can be observed in Figure 7.8. The *ASD* surface in Figure 8.8 has been shifted to a slightly higher α value, and the parabola describing the parabolic trough has been significantly narrowed (change in a_{eff} produces a larger change in α along trough). Also, the minimum has become much more pronounced for the surface corresponding to the larger initial frequency.

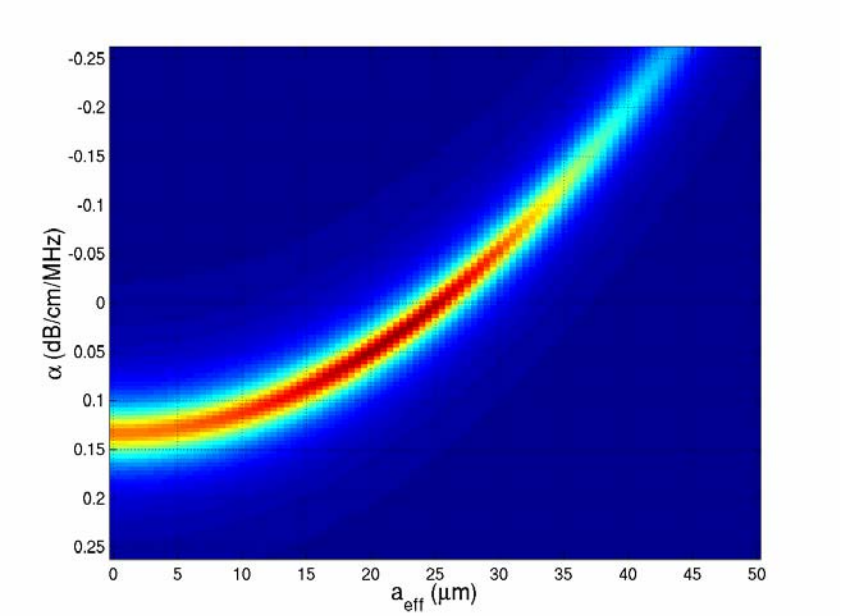

Figure 8.8: Example *ASD* surface for a half-space with an attenuation of 0 dB/cm/MHz containing 25 μm scatterers generated from 25 waveforms windowed with a 3 mm hamming window from a source whose filtering function $H(f)$ was given by Equation (7.4) using frequencies in the ka_{eff} range of 1.5 to 2.5. Dark red corresponds to a small *ASD* value and dark blue corresponds to a large *ASD* value. The minimum for this surface (dark red) occurs at a scatterer size of 21.9 μm.

Now the impact of the filtering characteristics of the source can be considered by generating the example *ASD* surface shown in Figure 8.9 for a source with filtering

characteristics given by Equation (7.1) with a σ_R of 18 MHz and a f_o of 8 MHz. All of the half-space and processing parameters will be the same as the surface shown in Figure 8.8, including the selection of frequencies corresponding to ka_{eff} values of 1.5 to 2.5. An initial ka_{eff} value of 1.5 corresponds to an initial frequency close to the top of the deviation peak (poor precision) for this source as can be observed in Figure 7.8. The parabola describing the parabolic trough has basically the same width and position in Figure 8.9 as in Figure 8.8. Also, the minimum is much less pronounced for the *ASD* surface shown in Figure 8.9 as compared to Figure 8.8 and is about as pronounced as the minimum in Figure 8.6. However, the reason for the peak being more pronounced in Figure 8.8 cannot be deduced based on a qualitative comparison of the different *ASD* surfaces.

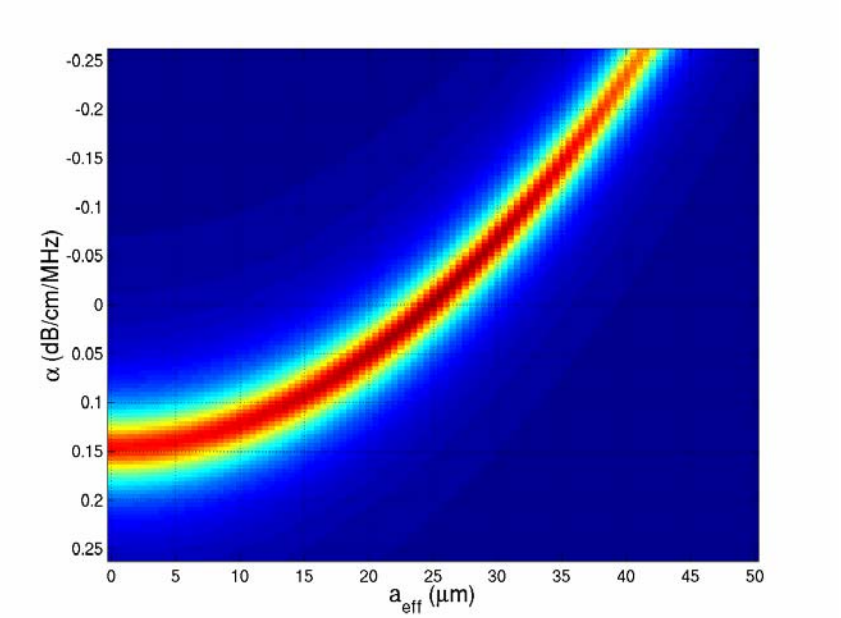

Figure 8.9: Example *ASD* surface for a half-space with an attenuation of 0 dB/cm/MHz containing 25 μm scatterers generated from 25 waveforms windowed with a 3 mm hamming window from a source whose filtering function $H(f)$ was given by Equation (7.1) with a σ_R of 18 MHz and a f_o of 8 MHz using frequencies in the ka_{eff} range of 1.5 to 2.5. Dark red corresponds to a small *ASD* value and dark blue corresponds to a large *ASD* value. The minimum for this surface (dark red) occurs at a scatterer size of 25.6 μm.

8.2 Mathematical Derivation and Analysis of Ideal *ASD* Surfaces

In the previous section, the impacts of attenuation, scatterer size, window length, frequency range, initial frequency, and source filtering function were investigated by looking at example *ASD* surfaces for some of the previously simulated waveforms. To better understand these example surfaces, a mathematical description of the surface is derived in this section. The

derivation can then be used to provide additional insight into the minimization of the *ASD* surface.

8.2.1 Derivation of ASD surface

To begin the derivation of the surface, assume the expression for $X(f,a_{eff},\alpha_o)$ from Equation (5.4) can be written as

$$\begin{aligned} X\left(f,a_{eff},\alpha_o\right) &= \ln\left(\frac{P_{scat}(f)}{\max_f\left(P_{scat}(f)\right)}\right) - \ln\left(\frac{P_{ref}(f)e^{-0.827\left(ka_{eff}\right)^2}e^{-4\alpha_o f z_T}}{\max_f\left(P_{ref}(f)e^{-0.827\left(ka_{eff}\right)^2}e^{-4\alpha_o f z_T}\right)}\right) \\ &= \ln\left(\frac{C_1 P_{ref}(f)\xi_s(f)e^{-0.827\left(ka_{real}\right)^2}e^{-4\alpha_{real} f z_T}}{\max_f\left(P_{scat}(f)\right)}\right) - \ln\left(\frac{P_{ref}(f)e^{-0.827\left(ka_{eff}\right)^2}e^{-4\alpha_o f z_T}}{\max_f\left(P_{ref}(f)e^{-0.827\left(ka_{eff}\right)^2}e^{-4\alpha_o f z_T}\right)}\right) \\ &= \ln\left(\xi_s(f)\right) - 0.827\left(\frac{2\pi}{c}\right)^2 f^2\left(a_{real}^2 - a_{eff}^2\right) - 4z_T\left(\alpha_{real}-\alpha_o\right)f + C_2, \end{aligned} \tag{8.1}$$

where C_1 and C_2 are constants independent of frequency related to the acoustic concentration and transmission coefficient for the intervening tissue layers, a_{real} and α_{real} are the real values of scatterer size and attenuation respectively, and $\xi_s(f)$ are the spectral fluctuations related to the random scatterer spacing. Hence, $\overline{X}$ becomes

$$\begin{aligned} \overline{X}\left(a_{eff},\alpha_o\right) = {} & \operatorname*{mean}_f\left[\ln\left(\xi_s(f)\right)\right] - 0.827\left(\frac{2\pi}{c}\right)^2\left(a_{real}^2 - a_{eff}^2\right)\operatorname*{mean}_f\left[f^2\right] \\ & - 4z_T\left(\alpha_{real}-\alpha_o\right)\operatorname*{mean}_f\left[f\right] + C_2 \end{aligned} \tag{8.2}$$

and

$$\begin{aligned} X - \overline{X} = {} & \left(\ln\left(\xi_s(f)\right) - \operatorname*{mean}_f\left[\ln\left(\xi_s(f)\right)\right]\right) - 0.827\left(\frac{2\pi}{c}\right)^2\left(a_{real}^2 - a_{eff}^2\right)\left(f^2 - \operatorname*{mean}_f\left[f^2\right]\right) \\ & - 4z_T\left(\alpha_{real}-\alpha_o\right)\left(f - \operatorname*{mean}_f\left[f\right]\right) \end{aligned} \tag{8.3}$$

yielding

$$
\begin{aligned}
\left(X-\overline{X}\right)^2 &= \left(\ln\left(\xi_s(f)\right)-\underset{f}{\text{mean}}\left[\ln\left(\xi_s(f)\right)\right]\right)^2 + 16z_T^2(\alpha_{real}-\alpha_o)^2\left(f-\underset{f}{\text{mean}}[f]\right)^2 \\
&+ 0.827^2\left(\frac{2\pi}{c}\right)^4\left(a_{real}^2-a_{eff}^2\right)^2\left(f^2-\underset{f}{\text{mean}}\left[f^2\right]\right)^2 \\
&+ 8z_T 0.827\left(\frac{2\pi}{c}\right)^2(\alpha_{real}-\alpha_o)\left(a_{real}^2-a_{eff}^2\right)\left(f-\underset{f}{\text{mean}}[f]\right)\left(f^2-\underset{f}{\text{mean}}\left[f^2\right]\right) \\
&- 2\left(\ln\left(\xi_s(f)\right)-\underset{f}{\text{mean}}\left[\ln\left(\xi_s(f)\right)\right]\right)0.827\left(\frac{2\pi}{c}\right)^2\left(a_{real}^2-a_{eff}^2\right)\left(f^2-\underset{f}{\text{mean}}\left[f^2\right]\right) \\
&- 2\left(\ln\left(\xi_s(f)\right)-\underset{f}{\text{mean}}\left[\ln\left(\xi_s(f)\right)\right]\right)4z_T(\alpha_{real}-\alpha_o)\left(f-\underset{f}{\text{mean}}[f]\right).
\end{aligned}
\tag{8.4}
$$

Therefore, the mean of $\left(X-\overline{X}\right)^2$ is given by

$$
\begin{aligned}
ASD &= \left(\underset{f}{\text{mean}}\left[\left(\ln\left(\xi_s(f)\right)\right)^2\right]-\left(\underset{f}{\text{mean}}\left[\ln\left(\xi_s(f)\right)\right]\right)^2\right) \\
&+ 0.827^2\left(\frac{2\pi}{c}\right)^4\left(a_{real}^2-a_{eff}^2\right)^2\left(\underset{f}{\text{mean}}\left[f^4\right]-\left(\underset{f}{\text{mean}}\left[f^2\right]\right)^2\right) \\
&+ 16z_T^2(\alpha_{real}-\alpha_o)^2\left(\underset{f}{\text{mean}}\left[f^2\right]-\left(\underset{f}{\text{mean}}[f]\right)^2\right) \\
&+ 8z_T 0.827\left(\frac{2\pi}{c}\right)^2(\alpha_{real}-\alpha_o)\left(a_{real}^2-a_{eff}^2\right)\left(\underset{f}{\text{mean}}\left[f^3\right]-\underset{f}{\text{mean}}[f]\underset{f}{\text{mean}}\left[f^2\right]\right) \\
&- 2\cdot 0.827\left(\frac{2\pi}{c}\right)^2\left(a_{real}^2-a_{eff}^2\right)\left(\underset{f}{\text{mean}}\left[f^2\ln\left(\xi_s(f)\right)\right]-\underset{f}{\text{mean}}\left[f^2\right]\underset{f}{\text{mean}}\left[\ln\left(\xi_s(f)\right)\right]\right) \\
&- 8z_T(\alpha_{real}-\alpha_o)\left(\underset{f}{\text{mean}}\left[f\ln\left(\xi_s(f)\right)\right]-\underset{f}{\text{mean}}[f]\underset{f}{\text{mean}}\left[\ln\left(\xi_s(f)\right)\right]\right).
\end{aligned}
\tag{8.5}
$$

Equation (8.5) could be simplified if $\ln(\xi_s(f))$ did not have any consistent dependence on frequency allowing $\underset{f}{\text{mean}}\left[f^2\ln\left(\xi_s(f)\right)\right]=\underset{f}{\text{mean}}\left[f^2\right]\underset{f}{\text{mean}}\left[\ln\left(\xi_s(f)\right)\right]$ and $\underset{f}{\text{mean}}\left[f\ln\left(\xi_s(f)\right)\right]=\underset{f}{\text{mean}}[f]\underset{f}{\text{mean}}\left[\ln\left(\xi_s(f)\right)\right]$. In order to determine if it is reasonable to assume that $\ln(\xi_s(f))$ is independent of frequency, the simulated backscattered waveforms generated for a half-space with an attenuation of 0 dB/cm/MHz containing 25 μm scatterers at a density of 35/mm^3 were considered. The source had filtering characteristics given by Equation (7.4). The waveforms were windowed in the time domain with a hamming window with a length of 3 mm. Once again, the 1000 waveforms were grouped into 40 sets of 25 waveforms, and the

25 waveforms in each set were averaged in the normal spectral domain to obtain 40 estimates for the P_{scat} versus frequency curves for frequencies corresponding to ka_{eff} values between 0.1 and 3. Each P_{scat} curve was then divided by $\max_f\left(P_{scat}(f)\right)P_{ref}(f)e^{-0.827(ka_{real})^2}e^{-4\alpha_{real}fz_T}$ and evaluated as a natural log in order to obtain 40 examples of $\ln(C_1\xi_s(f))$. These 40 examples were then averaged together and the resulting estimate of $\left(\ln\left(\xi_s(f)\right)-\underset{f}{\text{mean}}\left[\ln\left(\xi_s(f)\right)\right]\right)$ versus frequency was plotted in Figure 8.10. Clearly, on average $\ln(\xi_s(f))$ does not exhibit any consistent frequency dependence. As a result, Equation (8.5) can be simplified as

$$\begin{aligned} ASD = &\left(\underset{f}{\text{mean}}\left[\left(\ln\left(\xi_s(f)\right)\right)^2\right]-\left(\underset{f}{\text{mean}}\left[\ln\left(\xi_s(f)\right)\right]\right)^2\right) \\ &+0.827^2\left(\frac{2\pi}{c}\right)^4\left(a_{real}^2-a_{eff}^2\right)^2\left(\underset{f}{\text{mean}}\left[f^4\right]-\left(\underset{f}{\text{mean}}\left[f^2\right]\right)^2\right) \\ &+16z_T^2(\alpha_{real}-\alpha_o)^2\left(\underset{f}{\text{mean}}\left[f^2\right]-\left(\underset{f}{\text{mean}}\left[f\right]\right)^2\right) \\ &+8z_T 0.827\left(\frac{2\pi}{c}\right)^2(\alpha_{real}-\alpha_o)\left(a_{real}^2-a_{eff}^2\right)\left(\underset{f}{\text{mean}}\left[f^3\right]-\underset{f}{\text{mean}}\left[f\right]\underset{f}{\text{mean}}\left[f^2\right]\right). \end{aligned} \tag{8.6}$$

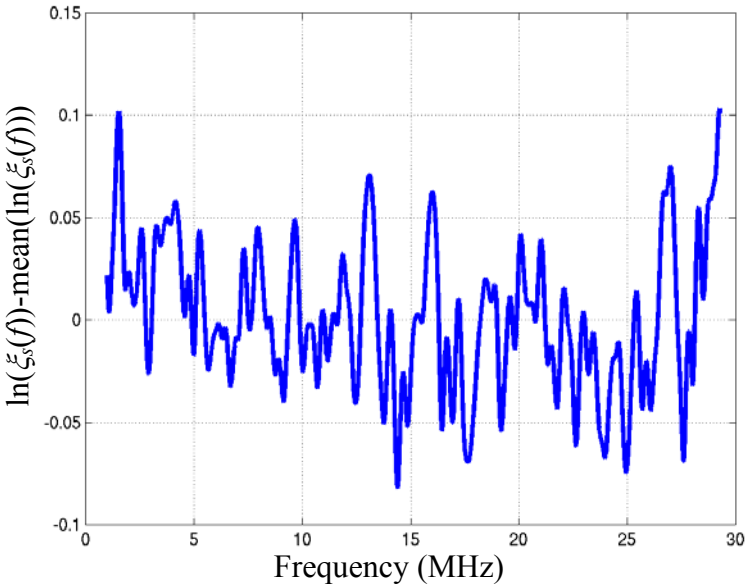

Figure 8.10: $\left(\ln\left(\xi_s(f)\right)-\underset{f}{\text{mean}}\left[\ln\left(\xi_s(f)\right)\right]\right)$ for waveforms from a half space with an attenuation of 0 dB/cm/MHz containing 25 μm scatterers at a density of 35/mm^3. The source had filtering characteristics given by Equation (7.4).

8.2.2 Analysis of ideal surfaces

After deriving Equation (8.6), the equation was used to calculate some ideal *ASD* surfaces. Initially, the parameters were selected to duplicate the results obtained using the simulated waveforms in order to validate our derivations. Then, the impact of each term in the summation of Equation (8.6) was evaluated. For all the calculated ideal *ASD* surfaces, z_T and c were the same as were used in the simulations for the *f*/4 source discussed previously.

The ideal *ASD* surfaces corresponding to half-spaces with 25 μm scatterers and attenuations of 0 dB/cm/MHz and 0.3 dB/cm/MHz are shown in Figures 8.11 and 8.12, respectively. Likewise, the ideal *ASD* surface for a half-space with 50 μm scatterers and an attenuation of 0 dB/cm/MHz is shown in Figure 8.13. The frequency range used when generating all three ideal surfaces was from 4.88 MHz to 14.6 MHz, corresponding to ka_{eff} values of 0.5 to 1.5 for the 25 μm scatterers and 1 to 3 for the 50 μm scatterers. Also, $\left(\underset{f}{\text{mean}}\left[\left(\ln\left(\xi_s(f) \right) \right)^2 \right] - \left(\underset{f}{\text{mean}}\left[\ln\left(\xi_s(f) \right) \right] \right)^2 \right)$ was set to a value of 0.03 that is comparable to the values found from analyzing some of the earlier simulation data (values varied from ~0.02 to ~0.08). Just as in the earlier surfaces from the simulation data, an increase in scatterer size and an increase in attenuation both shift the *ASD* surface to higher values of α. Also, the width of the parabola describing the parabolic trough is independent of both scatterer size and attenuation (change in a_{eff} produces the same change in α for all three surfaces). In addition, the minimum is much more pronounced for the larger scatterer size shown in Figure 8.13 as was also observed in the surfaces from the simulation data (Figures 8.3 and 8.4).

The impact of the total frequency range on the ideal *ASD* surface was also considered. Figure 8.14 shows an ideal surface calculated for a half-space with 50 μm scatterers and an attenuation of 0 dB/cm/MHz with $\left(\underset{f}{\text{mean}}\left[\left(\ln\left(\xi_s(f) \right) \right)^2 \right] - \left(\underset{f}{\text{mean}}\left[\ln\left(\xi_s(f) \right) \right] \right)^2 \right)$ still set to a value of 0.03. This time the frequency range extended from 4.88 MHz to 9.75 MHz corresponding to ka_{eff} values of 1 to 2. Once again, a decrease in the frequency range resulted in a less pronounced minimum, and the parabola describing the parabolic trough was broadened (change in a_{eff} produces smaller change in α along the trough).

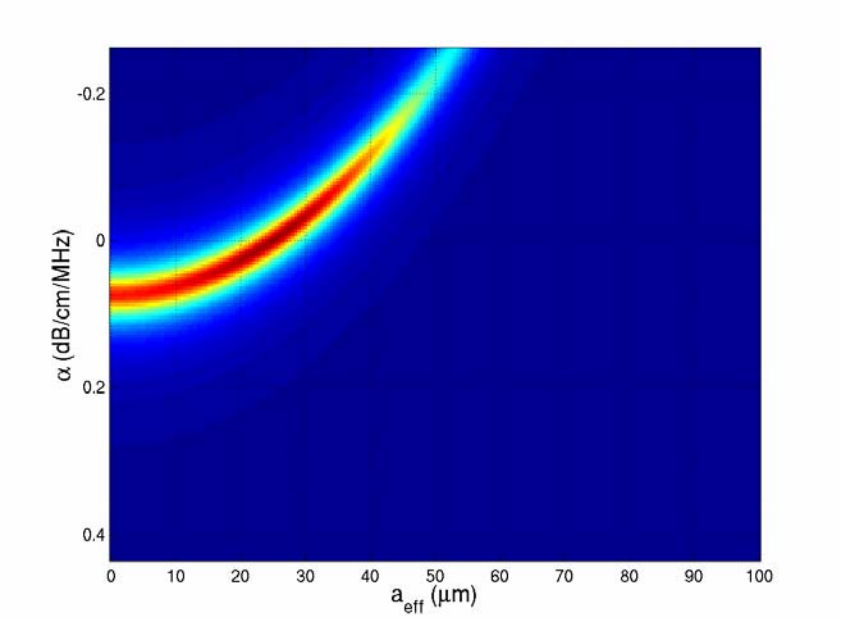

Figure 8.11: Ideal *ASD* surface for a half-space with an attenuation of 0 dB/cm/MHz containing 25 μm scatterers using frequencies in the ka_{eff} range of 0.5 to 1.5 for a $\left(\underset{f}{\text{mean}}\left[\left(\ln\left(\xi_s(f) \right) \right)^2 \right] - \left(\underset{f}{\text{mean}}\left[\ln\left(\xi_s(f) \right) \right] \right)^2 \right)$ value of 0.03. Dark red corresponds to a small *ASD* value and dark blue corresponds to a large *ASD* value.

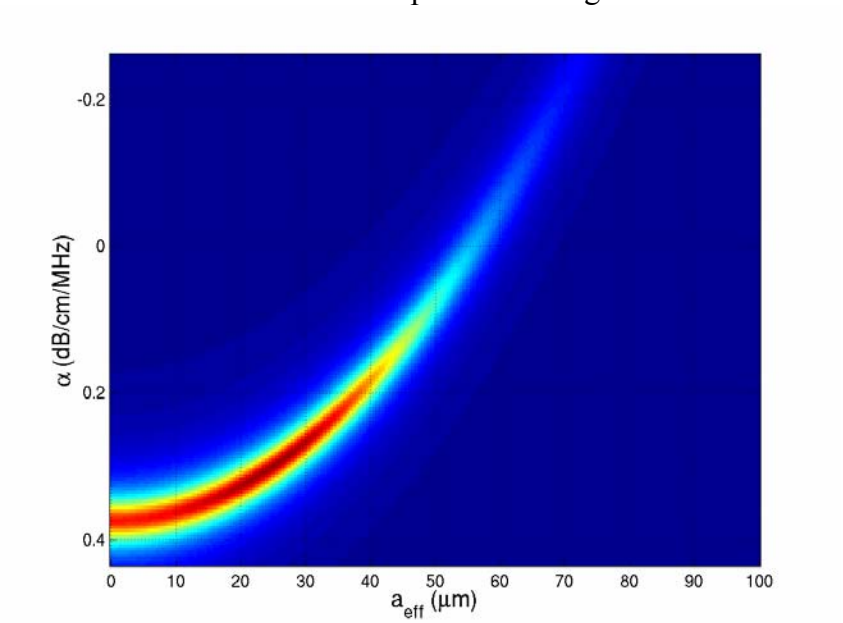

Figure 8.12: Ideal *ASD* surface for a half-space with an attenuation of 0.3 dB/cm/MHz containing 25 μm scatterers using frequencies in the ka_{eff} range of 0.5 to 1.5 for a $\left(\underset{f}{\text{mean}}\left[\left(\ln\left(\xi_s(f) \right) \right)^2 \right] - \left(\underset{f}{\text{mean}}\left[\ln\left(\xi_s(f) \right) \right] \right)^2 \right)$ value of 0.03. Dark red corresponds to a small *ASD* value and dark blue corresponds to a large *ASD* value.

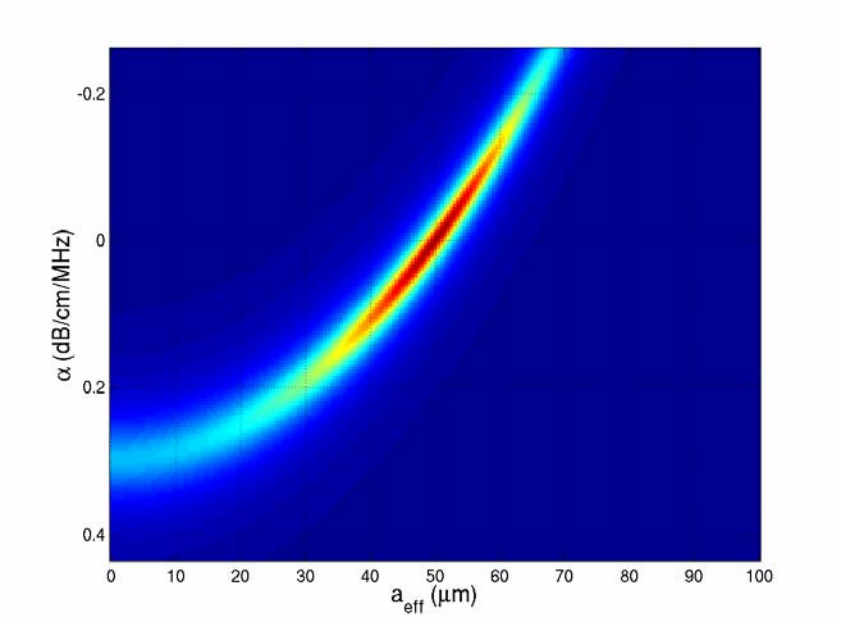

Figure 8.13: Ideal *ASD* surface for a half-space with an attenuation of 0 dB/cm/MHz containing 50 μm scatterers using frequencies in the ka_{eff} range of 1 to 3 for a $\left(\underset{f}{\text{mean}}\left[\left(\ln\left(\xi_s(f) \right) \right)^2 \right] - \left(\underset{f}{\text{mean}}\left[\ln\left(\xi_s(f) \right) \right] \right)^2 \right)$ value of 0.03. Dark red corresponds to a small *ASD* value and dark blue corresponds to a large *ASD* value.

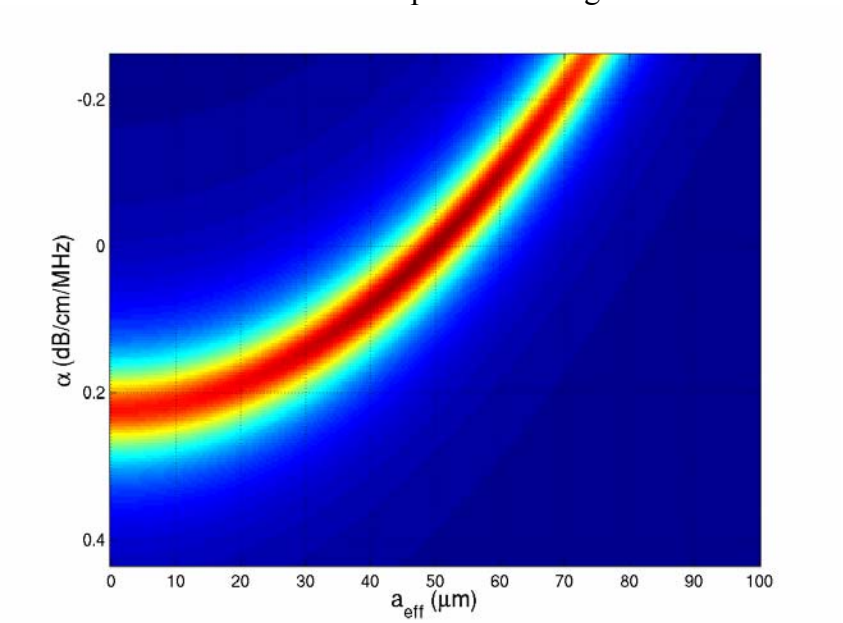

Figure 8.14: Ideal *ASD* surface for a half-space with an attenuation of 0 dB/cm/MHz containing 50 μm scatterers using frequencies in the ka_{eff} range of 1 to 2 for a $\left(\underset{f}{\text{mean}}\left[\left(\ln\left(\xi_s(f) \right) \right)^2 \right] - \left(\underset{f}{\text{mean}}\left[\ln\left(\xi_s(f) \right) \right] \right)^2 \right)$ value of 0.03. Dark red corresponds to a small *ASD* value and dark blue corresponds to a large *ASD* value.

Lastly, the impact of different initial frequencies on the ideal *ASD* surface was investigated. Figure 8.15 shows an ideal surface calculated for a half-space with 25 μm scatterers and an attenuation of 0 dB/cm/MHz with $\left(\underset{f}{\text{mean}}\left[\left(\ln\left(\xi_s(f) \right) \right)^2 \right] - \left(\underset{f}{\text{mean}}\left[\ln\left(\xi_s(f) \right) \right] \right)^2 \right)$ still set to a value of 0.03 and using frequencies from 14.6 MHz to 24.4 MHz (ka_{eff} values of 1.5 to 2.5). The parabola describing the parabolic trough has been narrowed (change in a_{eff} produces smaller change in α along the trough) for the larger initial frequency, just as had been observed in the analysis of the surfaces from the simulation data.

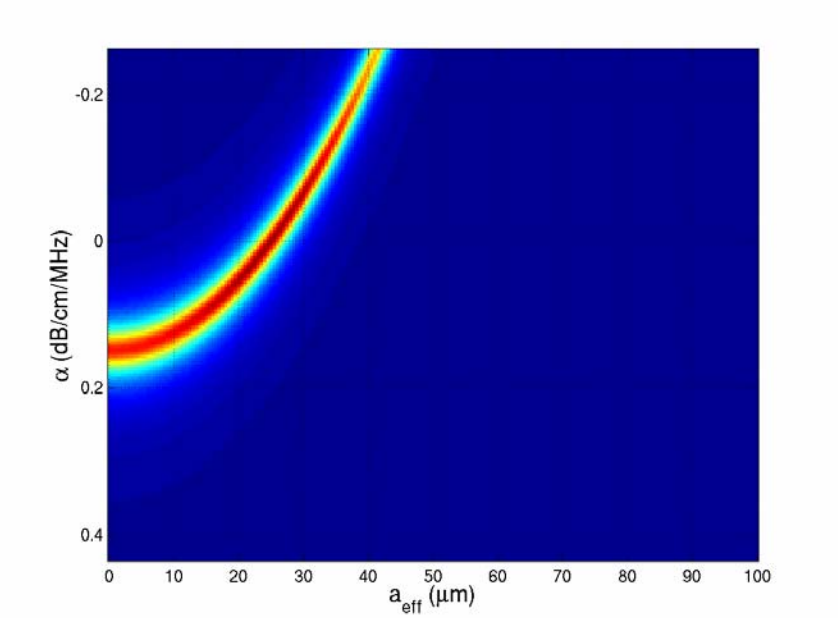

Figure 8.15: Ideal *ASD* surface for a half-space with an attenuation of 0 dB/cm/MHz containing 20 μm scatterers using frequencies in the ka_{eff} range of 1.5 to 2.5 for a $\left(\underset{f}{\text{mean}}\left[\left(\ln\left(\xi_s(f) \right) \right)^2 \right] - \left(\underset{f}{\text{mean}}\left[\ln\left(\xi_s(f) \right) \right] \right)^2 \right)$ value of 0.03. Dark red corresponds to a small *ASD* value and dark blue corresponds to a large *ASD* value.

Upon further comparison of Figure 8.15 to Figure 8.11, however, it is observed that peak has not been enhanced by using the larger initial frequency. Recall that in the analysis of the *ASD* surfaces from the simulation data, the peak was enhanced in Figure 8.8 ($H(f)$ by Equation (7.4), ka_{eff} of 1.5 to 2.5) where a larger initial frequency was used compared to the peak in Figure 8.6 ($H(f)$ by Equation (7.4), ka_{eff} of 0.5 to 1.5). However, the peak in Figure 8.9 ($H(f)$ by Equation (7.1), ka_{eff} of 1.5 to 2.5), which also had a larger initial frequency, was comparable to the peak in Figure 8.6. Therefore, there is some feature of the waveforms used to generate

Figure 8.8 that has not been captured by Equation (8.6) and that might also have been responsible for the improved precision at these frequencies for the source whose filtering function is given by Equation (7.4).

Even though the ideal *ASD* surface given by Equation (8.6) does not capture the dependence of the precision on the initial frequency on the high frequency end of the deviation peak, it still is able to capture all of the other dependencies observed in our analysis of the simulated waveforms. Therefore, the impact of each term in the summation of Equation (8.6) will be evaluated in order to provide further insights into the minimization surface of the Spectral Fit algorithm. The analysis was done by multiplying each term in the summation given by

$$\begin{aligned}
Term_{\xi} &= \left(\underset{f}{\text{mean}}\left[\left(\ln\left(\xi_s(f) \right) \right)^2 \right] - \left(\underset{f}{\text{mean}}\left[\ln\left(\xi_s(f) \right) \right] \right)^2 \right) \\
Term_{a_{eff}} &= 0.827^2 \left(\frac{2\pi}{c} \right)^4 \left(a_{real}^2 - a_{eff}^2 \right)^2 \left(\underset{f}{\text{mean}}\left[f^4 \right] - \left(\underset{f}{\text{mean}}\left[f^2 \right] \right)^2 \right) \\
Term_{\alpha} &= 16 z_T^2 \left(\alpha_{real} - \alpha_o \right)^2 \left(\underset{f}{\text{mean}}\left[f^2 \right] - \left(\underset{f}{\text{mean}}\left[f \right] \right)^2 \right) \\
Term_{\alpha, a_{eff}} &= 8 z_T 0.827 \left(\frac{2\pi}{c} \right)^2 \left(\alpha_{real} - \alpha_o \right) \left(a_{real}^2 - a_{eff}^2 \right) \left(\underset{f}{\text{mean}}\left[f^3 \right] - \underset{f}{\text{mean}}\left[f \right] \underset{f}{\text{mean}}\left[f^2 \right] \right)
\end{aligned} \tag{8.7}$$

by a factor independent of the other terms and then recalculating the ideal *ASD* surface (i.e., $ASD = Term_{\xi} + 1.01 \cdot Term_{a_{eff}} + Term_{\alpha} + Term_{\alpha, a_{eff}}$). The calculations were for a half-space with 50 μm scatterers and an attenuation of 0 dB/cm/MHz. The frequency range used when generating the surfaces was from 4.88 MHz to 14.6 MHz, corresponding to ka_{eff} values of 1 to 3. Also, $Term_{\xi}$ was set to a value of 0.03 except when evaluating its impact when it was given a value of 0.08.

First, consider the impact of $Term_{\xi}$ by comparing the new *ASD* surface corresponding to $Term_{\xi} = 0.08$ shown in Figure 8.16 to that shown in Figure 8.13, where $Term_{\xi} = 0.03$. The width of any given cross section of the parabolic trough is larger and the minimum is not as pronounced for the larger value of $Term_{\xi}$. However, the parabola describing the parabolic trough occurs at the same location along the α axis and has the same width (change in a_{eff} produces the same change in α along the trough) regardless of the amount of spectrum noise.

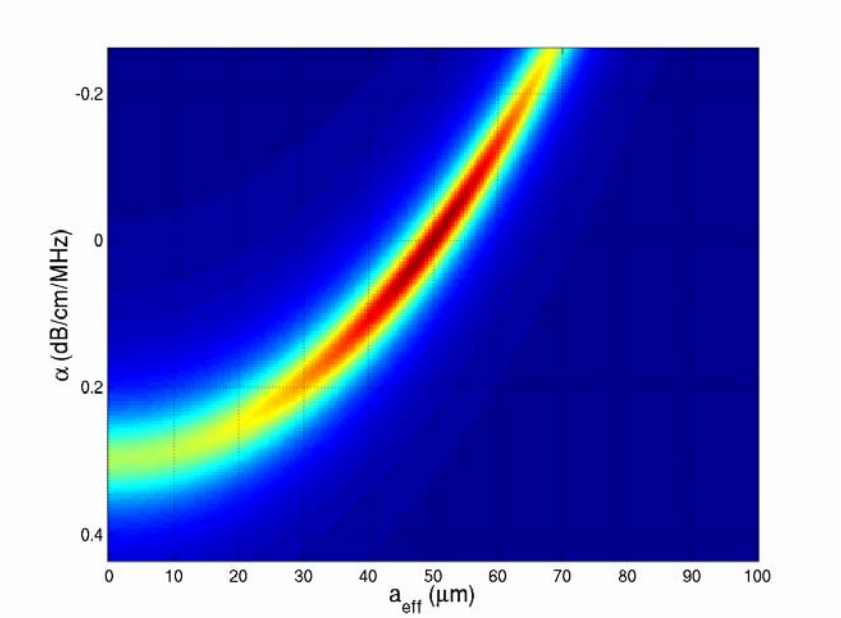

Figure 8.16: Ideal *ASD* surface to evaluate impact of $Term_{\xi}$ using a half-space with an attenuation of 0 dB/cm/MHz containing 50 μm scatterers using frequencies in the ka_{eff} range of 1 to 3 for $Term_{\xi} = 0.08$. Dark red corresponds to a small *ASD* value and dark blue corresponds to a large *ASD* value.

In Section 8.1, some observations were made regarding the relative importance of the minimum as half-space parameters, such as the scatterer size, and selected frequencies were varied for the simulated waveforms. However, the amount of spectral variation (i.e., $Term_{\xi}$) can vary for different waveform sets and frequencies for the same half-space depending upon the random arrangement of the scatterers. Since $Term_{\xi}$ can influence the relative importance of the minimum, the previous observations need to be validated by estimating $Term_{\xi}$ for each of the *ASD* plots from the simulated waveforms. The estimates for each of the surfaces were found by dividing each P_{scat} curve by $\max_{f}\left(P_{scat}(f)\right)P_{ref}(f)e^{-0.827(ka_{real})^2}e^{-4\alpha_{real}fz_T}$ to obtain an estimate of $\ln(C_1\xi(f))$ from which $Term_{\xi}$ was then calculated. The $Term_{\xi}$ values for all of the previous *ASD* curves for the simulated waveforms are given in Table 8.1. The $Term_{\xi}$ values for the simulated cases are all approximately the same except for Figure 8.7 that is significantly less. When we compared Figure 8.7 to 8.6 previously, the minimum of the *ASD* surface was less pronounced for the larger sized scatterers using the smaller frequency range (Figure 8.7). However, the smaller $Term_{\xi}$ value of Figure 8.7 should have resulted in a more pronounced minimum in the absence of

other effects. Hence, the previous observations regarding the prominence of the minimum in relation to the half-space parameters and selected frequencies are still valid.

Table 8.1: Estimates of $Term_{\xi}$ values for the *ASD* curves for the simulated waveforms.

Figure	8.1	8.2	8.3	8.4	8.5	8.6	8.7	8.8	8.9
$Term_{\xi}$	0.0380	0.0377	0.0366	0.0400	0.0426	0.0380	0.0203	0.0395	0.0354

Now consider the impact of $Term_{a_{eff}}$ and $Term_{\alpha}$ by comparing Figure 8.17, where $Term_{a_{eff}}$ was multiplied by a factor of 1.01, and Figure 8.18, where $Term_{\alpha}$ was multiplied by a factor of 1.01, to Figure 8.13. Figures 8.17 and 8.18 are indistinguishable, with the minimum being much more pronounced than the minimum in Figure 8.13. However, the parabola describing the parabolic trough occurs at the same location and has the same width (change in a_{eff} produces the same change in α along the trough) for all three figures.

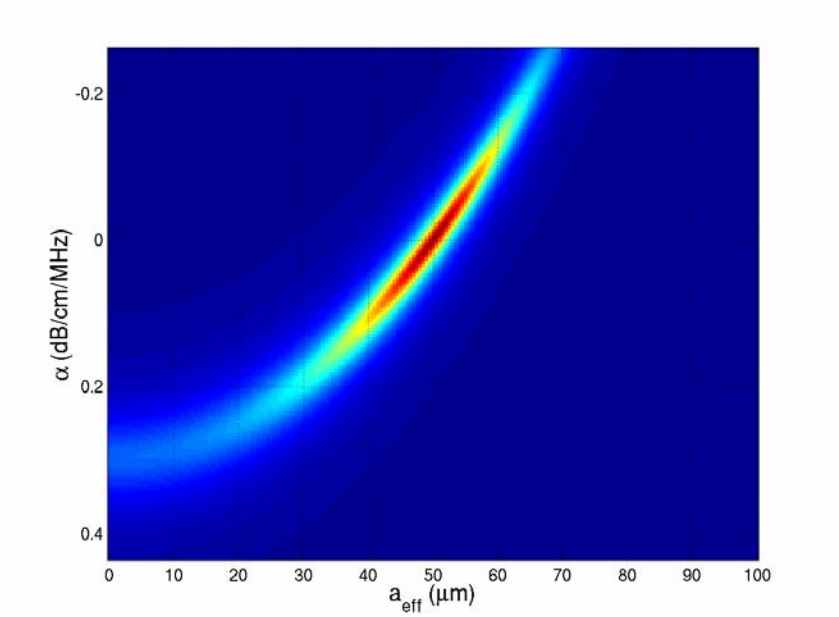

Figure 8.17: Ideal *ASD* surface to evaluate impact of $1.01 \cdot Term_{a_{eff}}$ using a half-space with an attenuation of 0 dB/cm/MHz containing 50 μm scatterers using frequencies in the ka_{eff} range of 1 to 3 for $Term_{\xi} = 0.03$. Dark red corresponds to a small *ASD* value and dark blue corresponds to a large *ASD* value.

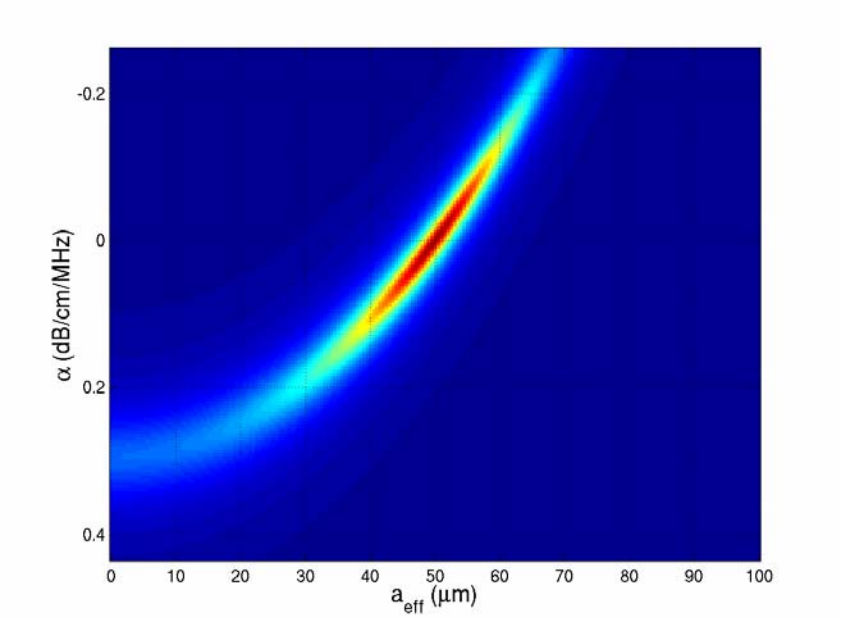

Figure 8.18: Ideal *ASD* surface to evaluate impact of $1.01 \cdot Term_{\alpha}$ using a half-space with an attenuation of 0 dB/cm/MHz containing 50 μm scatterers using frequencies in the ka_{eff} range of 1 to 3 for $Term_{\xi} = 0.03$. Dark red corresponds to a small *ASD* value and dark blue corresponds to a large *ASD* value.

The impact of $Term_{\alpha,a_{eff}}$ can now be analyzed by comparing Figure 8.13 to Figures 8.19 and 8.20 where $Term_{\alpha,a_{eff}}$ has been multiplied by factors of 1.005 and 1.008, respectively. The parabola describing the parabolic trough occurs at the same location and has the same width (change in a_{eff} produces the same change in α along the trough). However, the minimum is less pronounced as the factor multiplying $Term_{\alpha,a_{eff}}$ is increased from 1 (Figure 8.13), to 1.005 (Figure 8.19), and then to 1.008 (Figure 8.20). Also, the degradation of the minimum is more severe for larger $Term_{\alpha,a_{eff}}$ than for smaller $Term_{a_{eff}}$ or $Term_{\alpha}$ for the same percent change. Hence, increasing $Term_{a_{eff}}$ or $Term_{\alpha}$ may not enhance the minimum if $Term_{\alpha,a_{eff}}$ is also increased at the same time. Also, the existence of the parabolic trough can be attributed to $Term_{\alpha,a_{eff}}$ because the minimum is less pronounced as this term increases.

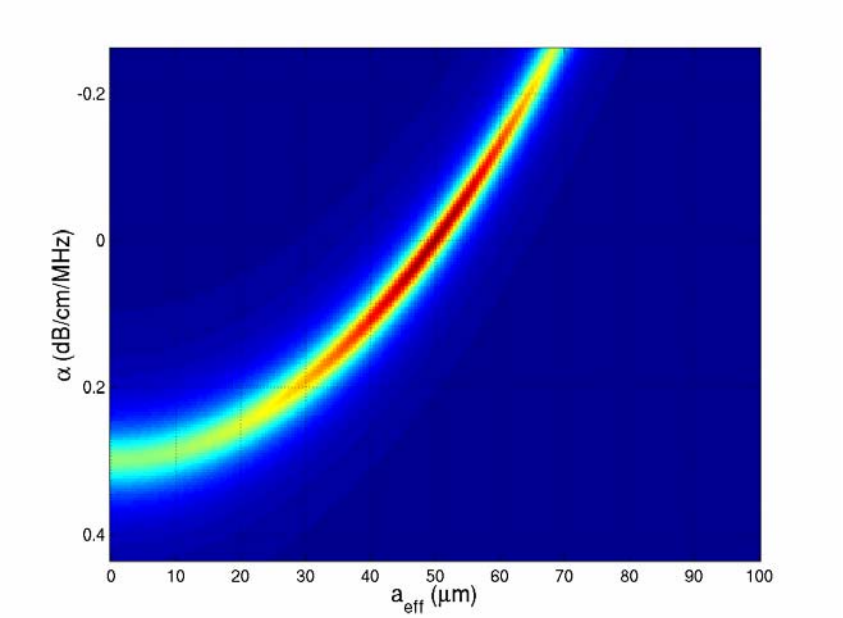

Figure 8.19: Ideal *ASD* surface to evaluate impact of $1.005 \cdot Term_{\alpha,a_{eff}}$ using a half-space with an attenuation of 0 dB/cm/MHz containing 50 μm scatterers using frequencies in the ka_{eff} range of 1 to 3 for $Term_{\xi} = 0.03$. Dark red corresponds to a small *ASD* value and dark blue corresponds to a large *ASD* value.

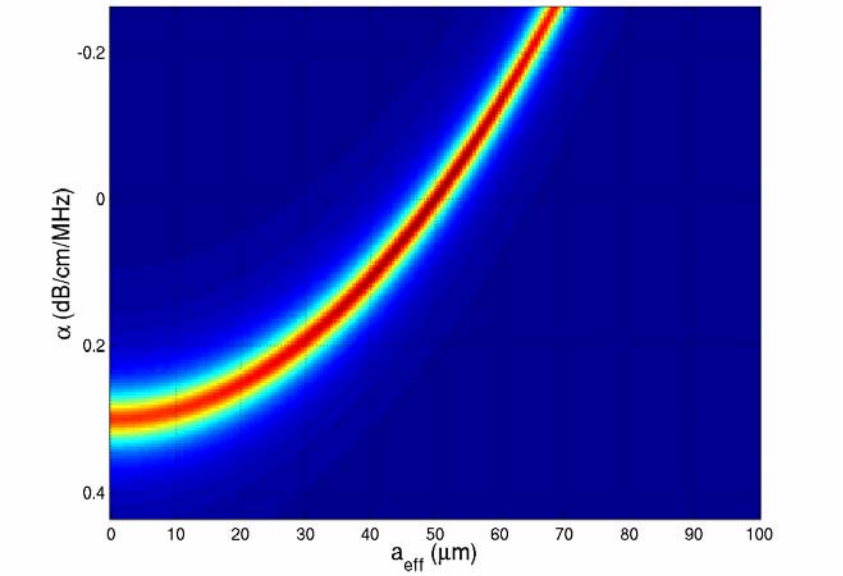

Figure 8.20: Ideal *ASD* surface to evaluate impact of $1.008 \cdot Term_{\alpha,a_{eff}}$ using a half-space with an attenuation of 0 dB/cm/MHz containing 50 μm scatterers using frequencies in the ka_{eff} range of 1 to 3 for $Term_{\xi} = 0.03$. Dark red corresponds to a small *ASD* value and dark blue corresponds to a large *ASD* value.

8.3 Relating Properties of the *ASD* Surfaces to Precision of Spectral Fit Algorithm

In the previous sections, changes to the *ASD* surface were observed for different scatterer sizes, half-space attenuations, spectral variance (i.e., $Term_{\xi}$), frequency ranges, and initial frequencies. It was observed that the minimum of the *ASD* surface became more pronounced for larger Δka_{eff} ranges for the same frequency range (Figures 8.2, 8.3, 8.4, 8.11, and 8.13), for larger Δka_{eff} ranges for the same scatterer size (Figures 8.13 and 8.14), for the same Δka_{eff} ranges for larger frequency ranges (Figures 8.6, 8.7, 8.11, and 8.14), and for smaller spectral variances (Figures 8.13 and 8.16). Also, the parabola describing the parabolic trough of the *ASD* surface was narrowed for the same Δka_{eff} range with larger frequency ranges (Figures 8.6, 8.7, 8.11, and 8.14) and for the same Δka_{eff} range and frequency range with larger initial frequency (Figures 8.6, 8.9, 8.15, and 8.11). However, these changes of the *ASD* surfaces have not been related to the precision of the Spectral Fit algorithm. In addition, the ideal *ASD* surfaces in Section 8.2 always had a minimum at the correct location even as the overall shape of the *ASD* surface was altered by the different half-space parameters and frequency ranges. Hence, the first step is to determine the cause of inaccuracies in the estimate. The impact of the causes can then be addressed as the *ASD* surfaces are changed.

The most likely cause of inaccuracies in the estimate is $\ln(\xi_s(f))$ having some frequency dependence for some set of waveforms. This would not contradict the results presented in Figure 8.10 because on average $\ln(\xi_s(f))$ would have no frequency dependence yielding accurate average estimates as was observed in the earlier chapters. In order to explore this possibility, values for

$$\begin{aligned}\sigma_{f^2,\xi} &= \left(\underset{f}{\text{mean}}\left[f^2 \ln\left(\xi_s(f)\right)\right] - \underset{f}{\text{mean}}\left[f^2\right]\underset{f}{\text{mean}}\left[\ln\left(\xi_s(f)\right)\right]\right) \\ \sigma_{f,\xi} &= \left(\underset{f}{\text{mean}}\left[f \ln\left(\xi_s(f)\right)\right] - \underset{f}{\text{mean}}\left[f\right]\underset{f}{\text{mean}}\left[\ln\left(\xi_s(f)\right)\right]\right)\end{aligned} \tag{8.7}$$

were estimated for some of the simulated waveforms along with the corresponding $Term_{\xi}$. These values were then input into Equation (8.5) with the same half-space parameters and frequency range that had been used to generate and obtain estimates for the simulated waveforms in order to generate a corresponding *ASD* surface. When generating the surfaces, a_{eff} was varied from 0 μm to 50 μm in steps of 0.02 μm while α was varied from –0.174 dB/cm/MHz to 0.174 dB/cm/MHz in steps of .000869 dB/cm/MHz. The true scatterer size used in the simulation was 25 μm and the true half-space attenuation was 0 dB/cm/MHz. A scatterer size was then

determined by finding the minimum of the generated *ASD* surface. The scatterer size from the generated surface was then compared to the scatterer size given by the Spectral Fit algorithm for the same set of waveforms. The comparison of the two scatterer sizes along with the estimated values of $Term_{\xi}$, $\sigma_{f^2,\xi}$, and $\sigma_{f,\xi}$ are given in Table 8.2. The first three rows correspond to the data sets used to generate Figures 8.6, 8.8, and 8.9, respectively. The minimum value of the generated *ASD* surface has also been provided.

The values for the scatterer size from the generated *ASD* surface are in good agreement with the scatterer sizes from the Spectral Fit algorithm for the same data set for all of the cases except for the data set corresponding to Figure 8.8 (i.e., 21.9 μm from the Spectral Fit algorithm compared to 0 μm from the *ASD* surface). The discrepancy for the Figure 8.8 data set is another indication that the current theory cannot account for the deviation peak discussed in Section 7.3. The agreement for the other data sets would probably be further enhanced if smaller step sizes were used to generate the *ASD* surface. Because when larger step sizes of 0.5 μm and 0.00434 dB/cm/MHz were used to generate an *ASD* for the first case in Table 8.2, the scatterer size estimate was 19.5 μm instead of 19.1 μm. Hence, the errors in the estimates from the Spectral Fit algorithm are due to the finite values of $\sigma_{f^2,\xi}$ and $\sigma_{f,\xi}$ due to the good agreement in a_{eff} from the Spectral Fit algorithm and the generated *ASD* surface. In addition, the inclusion of $\sigma_{f^2,\xi}$ and $\sigma_{f,\xi}$ in Equation (8.5) reduces the *ASD* value below the ideal minimum of $Term_{\xi}$ with a greater reduction for the poorer estimates. It may be possible to exploit this effect in a new minimization algorithm if an accurate estimate of $Term_{\xi}$ could be obtained for any given data set.

Table 8.2: Comparison between the scatterer size from the generated surface and the scatterer size given by the Spectral Fit algorithm for the same data set along with the minimum value of the generated ASD surface as well as the estimated values of $Term_{\xi}$, $\sigma_{f^2,\xi}$, and $\sigma_{f,\xi}$.

a_{eff} from Spectral Fit Algorithm	a_{eff} from Generated *ASD* Surface	$Term_{\xi}$	Minimum of Generated *ASD* Surface	$\sigma_{f^2,\xi}$	$\sigma_{f,\xi}$
18.4 μm	19.1 μm	0.0380	0.0371	-0.502	-0.0362
21.9 μm	0 μm	0.0395	0.0312	-1.364	-0.0529
25.6 μm	25.7 μm	0.0354	0.0351	1.715	0.0447
.0360 nm	0 μm	0.0359	0.0277	-1.062	-0.0451
29.2 μm	28.7 μm	0.0264	0.0232	5.786	0.1523
29.3 μm	29.0 μm	0.0317	0.0308	-2.535	-0.0608
37.4 μm	36.5 μm	0.0368	0.0307	2.520	0.0786

Once the causes of the errors in the estimate were known to be the finite values of $\sigma_{f^2,\xi}$ and $\sigma_{f,\xi}$, the effect of these terms on the overall *ASD* surface was investigated. The investigation was done using the ideal *ASD* surface corresponding to a half-space with 50 μm scatterers and an attenuation of 0 dB/cm/MHz using frequencies in the ka_{eff} range of 1 to 3 (i.e. Figure 8.13) with a $Term_{\xi}$ of 0.03. The ideal surface was generated four times corresponding to $\sigma_{f^2,\xi}=1$ with $\sigma_{f,\xi}=0$, $\sigma_{f^2,\xi}=-1$ with $\sigma_{f,\xi}=0$, $\sigma_{f^2,\xi}=0$ with $\sigma_{f,\xi}=0.05$, and $\sigma_{f^2,\xi}=0$ with $\sigma_{f,\xi}=-0.05$, shown in Figures 8.21-8.24, respectively. The impact of each case was then assessed by comparing the generated figures to Figure 8.13 where both $\sigma_{f^2,\xi}$ and $\sigma_{f,\xi}$ were zero.

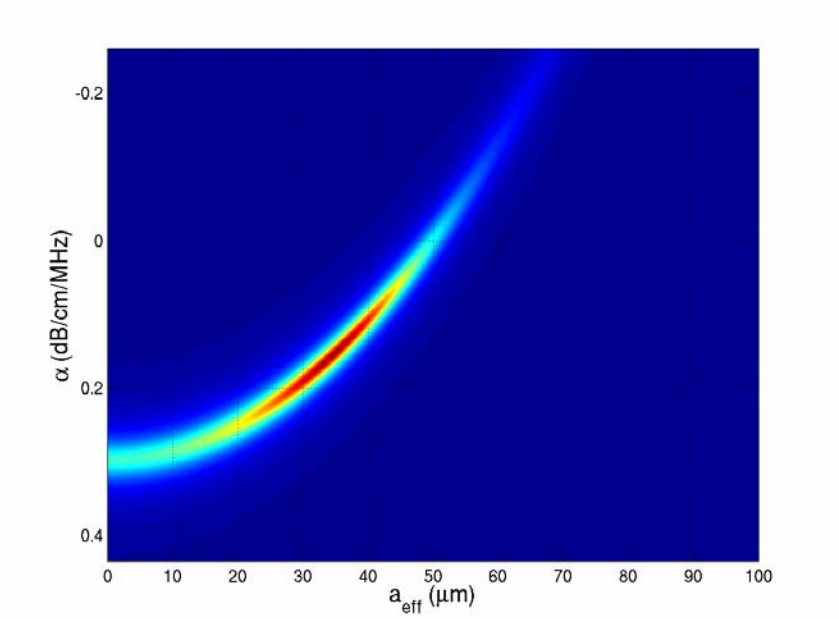

Figure 8.21: Ideal *ASD* surface for a half-space with an attenuation of 0 dB/cm/MHz containing 50 μm scatterers using frequencies in the ka_{eff} range of 1 to 3 for a $Term_{\xi}$ of 0.03 with $\sigma_{f^2,\xi}=1$ and $\sigma_{f,\xi}=0$. The new minimum corresponds to a scatterer size of 34.62 μm. Dark red corresponds to a small *ASD* value and dark blue corresponds to a large *ASD* value.

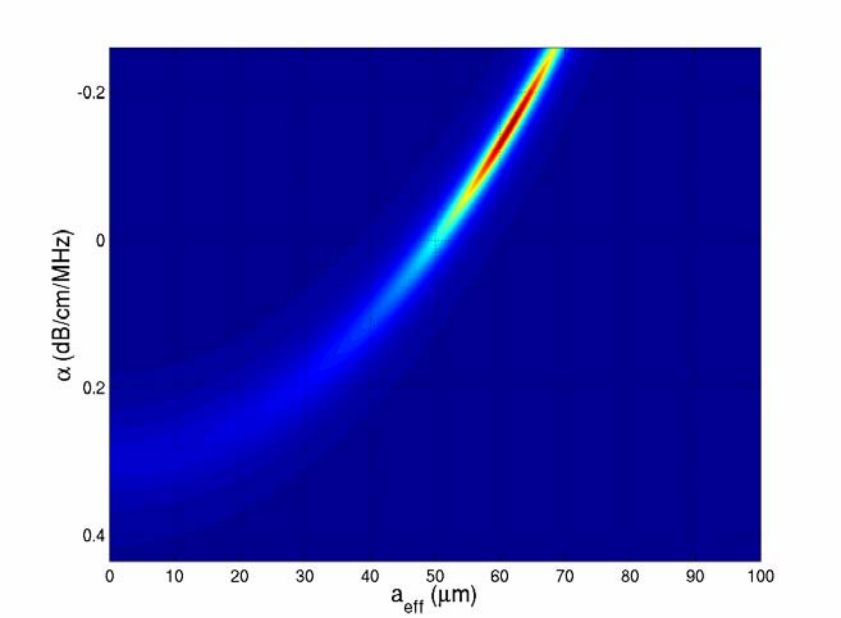

Figure 8.22: Ideal *ASD* surface for a half-space with an attenuation of 0 dB/cm/MHz containing 50 μm scatterers using frequencies in the ka_{eff} range of 1 to 3 for a $Term_{\xi}$ of 0.03 with $\sigma_{f^2,\xi} = -1$ and $\sigma_{f,\xi} = 0$. The new minimum corresponds to a scatterer size of 61.66 μm. Dark red corresponds to a small *ASD* value and dark blue corresponds to a large *ASD* value.

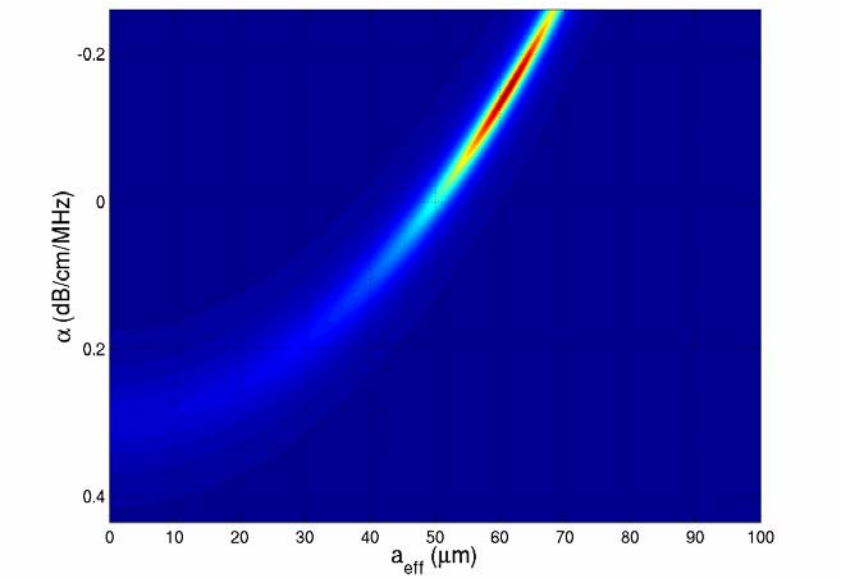

Figure 8.23: Ideal *ASD* surface for a half-space with an attenuation of 0 dB/cm/MHz containing 50 μm scatterers using frequencies in the ka_{eff} range of 1 to 3 for a $Term_{\xi}$ of 0.03 with $\sigma_{f^2,\xi} = 0$ and $\sigma_{f,\xi} = 0.05$. The new minimum corresponds to a scatterer size of 61.36 μm. Dark red corresponds to a small *ASD* value and dark blue corresponds to a large *ASD* value.

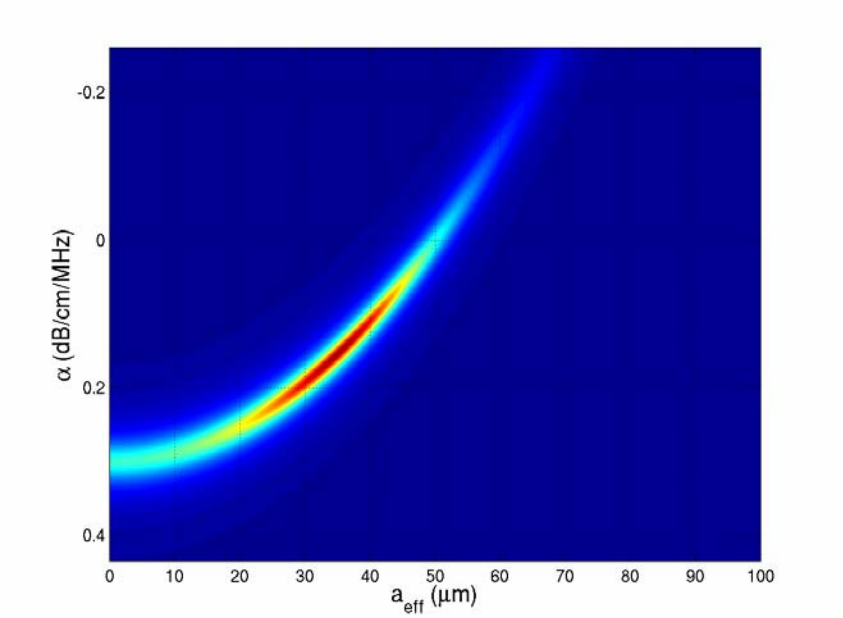

Figure 8.24: Ideal *ASD* surface for a half-space with an attenuation of 0 dB/cm/MHz containing 50 μm scatterers using frequencies in the ka_{eff} range of 1 to 3 for a $Term_{\xi}$ of 0.03 with $\sigma_{f^2,\xi} = 0$ and $\sigma_{f,\xi} = -0.05$. The new minimum corresponds to a scatterer size of 35.14 μm. Dark red corresponds to a small *ASD* value and dark blue corresponds to a large *ASD* value.

In all four figures, the parabola describing the parabolic trough occurs at the same location and has the same width as the parabola describing the parabolic trough in Figure 8.13. However, the minimum occurs at different locations along the trough for the different values of $\sigma_{f^2,\xi}$ and $\sigma_{f,\xi}$. A $\sigma_{f^2,\xi}$ of 1 with a $\sigma_{f,\xi}$ of 0 (Figure 8.21) and a $\sigma_{f^2,\xi}$ of 0 with a $\sigma_{f,\xi}$ of –0.05 (Figure 8.24) shift the minimum to a lower scatterer size and larger attenuation, while a $\sigma_{f^2,\xi}$ of -1 with a $\sigma_{f,\xi}$ of 0 (Figure 8.22) and a $\sigma_{f^2,\xi}$ of 0 with a $\sigma_{f,\xi}$ of 0.05 (Figure 8.23) shift the minimum to a larger scatterer size and smaller attenuation. Hence, for the same sign, $\sigma_{f^2,\xi}$ and $\sigma_{f,\xi}$ shift the minimum in opposite directions. Because $\sigma_{f^2,\xi}$ and $\sigma_{f,\xi}$ typically have the same sign, as is indicated by the results in Table 8.2, the two frequency dependencies will counterbalance each other. In addition, for the same magnitude of $\sigma_{f^2,\xi}$ and $\sigma_{f,\xi}$, the shift to smaller scatterer sizes appears to result in a larger percentage error in the new location of the minimum. Upon examining Figure 8.13, it is clear that the *ASD* curve increases slightly faster as the parabolic trough moves to larger scatterer sizes away from the minimum as opposed to

moving to smaller scatterer sizes. Hence, the error introduced by the frequency dependence of $\ln(\xi_s(f))$ appears to be limited by the rate of change of the original *ASD* surface.

A more detailed comparison reveals that the minimum is slightly more pronounced for Figures 8.21 and 8.24, which are comparable, than for Figure 8.13, and the minimum is even more pronounced for Figures 8.23 and 8.22, which are also comparable. Hence, the enhancement of the minimum appears to be related to the rate of change of the original *ASD* surface before the frequency dependence of $\ln(\xi_s(f))$ has been included as well. In order to clarify the effect of the shift on the prominence of the minimum, consider the ideal surface shown in Figure 8.25 where $\sigma_{f^2,\xi} = 0$ with $\sigma_{f,\xi} = -0.025$. In Figure 8.25, the minimum is comparable to the minimum in Figure 8.13 and has not been shifted as far away from the true scatterer size and attenuation as the minimum in Figure 8.24. Hence, the enhancement of the minimum also appears to be related to the amount the minimum has been shifted away from its true value.

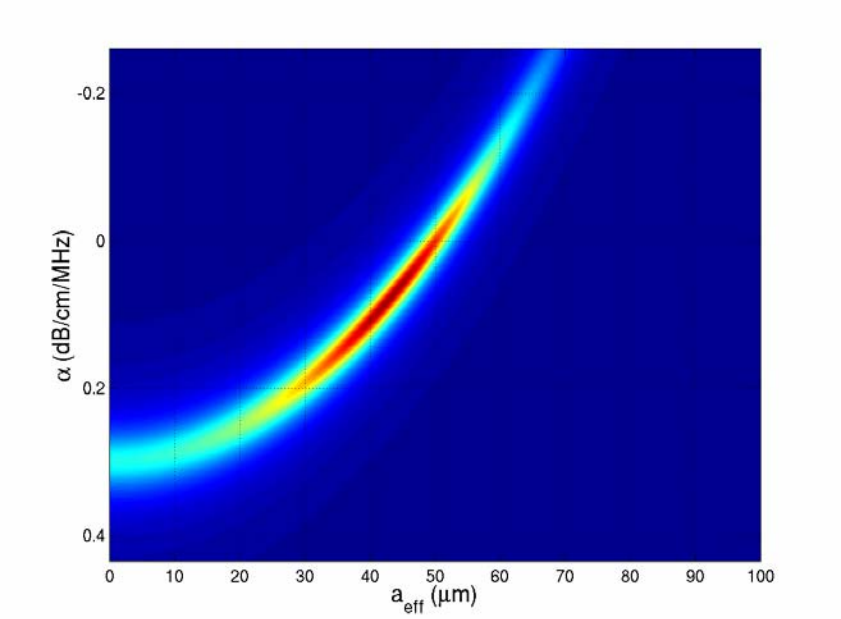

Figure 8.25: Ideal *ASD* surface for a half-space with an attenuation of 0 dB/cm/MHz containing 50 μm scatterers using frequencies in the ka_{eff} range of 1 to 3 for a $Term_{\xi}$ of 0.03 with $\sigma_{f^2,\xi} = 0$ and $\sigma_{f,\xi} = -0.025$. The new minimum corresponds to a scatterer size of 43.22 μm. Dark red corresponds to a small *ASD* value and dark blue corresponds to a large *ASD* value.

Now that the error in the estimation scheme has been related to the shift in the minimum of the *ASD* surface away from the true value, the dependence of the shift on the properties of the ideal *ASD* surface for any given data set can be explored. Consider the *ASD* surfaces shown in Figures 8.26 and 8.27. Both surfaces were generated for a half-space with 50 μm scatterers and an attenuation of 0 dB/cm/MHz with $Term_{\xi}$ of 0.03, $\sigma_{f^2,\xi}$ of -1, and $\sigma_{f,\xi}$ of 0. However, in Figure 8.26 the minimum was enhanced by multiplying $Term_{\alpha}$ by 1.01, and the calculation involved frequencies in the ka_{eff} range of 1 to 3. Likewise, in Figure 8.27 the parabola describing the parabolic trough was broadened by using frequencies in the ka_{eff} range of 0.01 to 2.01. Upon comparing Figure 8.26 to Figure 8.22, it is clear that the minimum has been shifted by a smaller amount when the minimum of the original surface (prior to inclusion of $\sigma_{f^2,\xi}$) is more pronounced. Hence, the precision of the estimates should be improved when the minimum of the *ASD* surface is better defined. The minimum was better defined when the Δka_{eff} or frequency range was increased. Therefore, the increased precision with increased frequency range and Δka_{eff} range observed in Chapter 7 agrees with our analysis of the *ASD* surface.

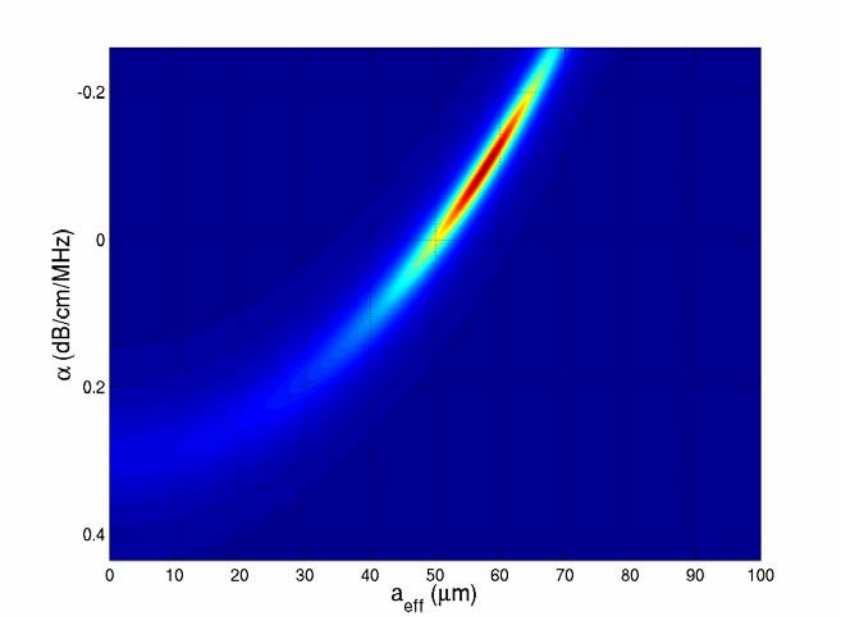

Figure 8.26: Ideal *ASD* surface for a half-space with an attenuation of 0 dB/cm/MHz containing 50 μm scatterers using frequencies in the ka_{eff} range of 1 to 3 for a $Term_{\xi}$ of 0.03 with $\sigma_{f^2,\xi} = -1$ and $\sigma_{f,\xi} = 0$ while enhancing the minimum by multiplying $Term_{\alpha}$ by 1.01. The new minimum corresponds to a scatterer size of 57.68 μm. Dark red corresponds to a small *ASD* value and dark blue corresponds to a large *ASD* value.

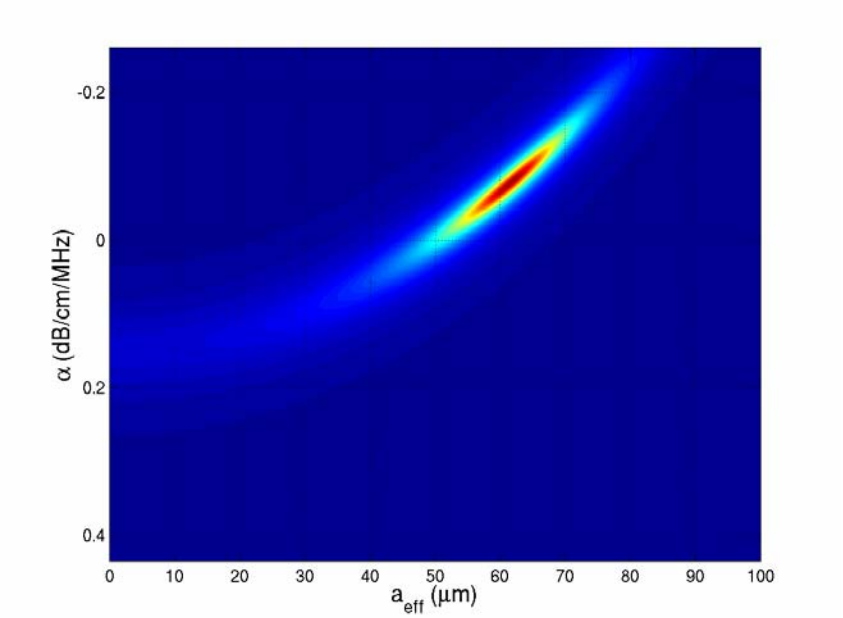

Figure 8.27: Ideal *ASD* surface for a half-space with an attenuation of 0 dB/cm/MHz containing 50 μm scatterers using frequencies in the ka_{eff} range of 0.01 to 2.01 for a $Term_{\xi}$ of 0.03 with $\sigma_{f^2,\xi} = -1$ and $\sigma_{f,\xi} = 0$. The new minimum corresponds to a scatterer size of 61.66 μm. Dark red corresponds to a small *ASD* value and dark blue corresponds to a large *ASD* value.

Now compare Figure 8.27 to Figure 8.22. The error in the scatterer size is the same for both surfaces. However, because the parabola describing the parabolic trough is broader in Figure 8.27, the corresponding error in the half-space attenuation is less (-0.0782 dB/cm/MHz as compared to –0.1546 dB/cm/MHz). Therefore, broadening the parabola describing the parabolic trough should improve the precision of the attenuation estimate while not affecting the scatterer size estimate. Hence, the precision of the attenuation estimate should be reduced as we increase the initial frequency without changing the precision of the size estimate, as was also observed for the initial frequencies below the deviation peak in Chapter 7. The frequencies above the deviation peak were shown to have a more pronounced minimum in Figure 8.8 that cannot be accounted for using the current *ASD* theory.

Before concluding, one case needs to be considered in greater detail. Recall that in Chapter 7, an increase in the frequency range for the same Δka_{eff} range improved the precision of the attenuation estimate while maintaining the same precision for the scatterer size estimate. However, in this chapter, the parabola describing the parabolic trough of the *ASD* surface was noted to be narrower for the larger frequency range (Figures 8.6, 8.7, 8.11, and 8.14). Hence, for the same error in scatterer size (in μm), the narrower parabola would have resulted in a larger

error in the attenuation estimate. This apparent discrepancy can be reconciled by recalling that it was the same percent error in scatterer size that resulted in the improved precision for the attenuation estimate for the larger frequency ranges. The same percent change in scatterer size in Figure 8.14 and Figure 8.7 still produces a larger change in the attenuation along the parabolic trough than the corresponding percent change in Figure 8.11 and Figure 8.6. Hence, the observations regarding the *ASD* surface for this case agree with the results presented in Chapter 7.

8.4 Chapter Summary

In this chapter, an analysis was performed of the *ASD* surface over which the Spectral Fit algorithm finds the minimum when estimating the scatterer size and total attenuation. The analysis was done using both the simulated waveforms from the earlier chapters as well as ideal surfaces corresponding to a derived expression for the *ASD* surface. The surface was found to have a single minimum that always occurred along a parabolic trough. The existence of the parabolic trough could be attributed to a cross term between the attenuation and scatterer size minimizations, $Term_{\alpha, a_{eff}}$.

Also, it was observed that the minimum of the *ASD* surface became more pronounced for larger Δka_{eff} ranges for the same frequency range (Figures 8.2, 8.3, 8.4, 8.11, and 8.13), for larger Δka_{eff} ranges for the same scatterer size (Figures 8.13 and 8.14), for the same Δka_{eff} ranges for larger frequency ranges (Figures 8.6, 8.7, 8.11, and 8.14), and for smaller spectral variances (Figures 8.13 and 8.16). Also, the parabola describing the parabolic trough of the *ASD* surface was narrowed for the same Δka_{eff} range with larger frequency ranges (Figures 8.6, 8.7, 8.11, and 8.14) and for the same Δka_{eff} range and frequency range with larger initial frequency (Figures 8.6, 8.9, 8.15, and 8.11). The shift of the minimum along the parabolic trough away from its true value was then related to the frequency dependence of the spectral variations resulting from the random scatterer spacing, $\ln(\xi_s(f))$. For the same frequency dependence of $\ln(\xi_s(f))$, the shift of the minimum away from the true value was found to be reduced (improvement in precision) when the minimum of the surface was more pronounced. In addition, the error in the half-space attenuation due to the shift in the minimum is less when the parabola describing the parabolic trough is broader (all other terms remaining the same). Hence, the analysis of the *ASD* surface is in agreement with the results presented in Chapter 7 regarding

Δka_{eff} range, frequency range, and initial frequencies below the deviation peak. The results for initial frequencies greater than the deviation peak were found to not be consistent with *ASD* analysis, once again indicating a limitation in the current theory or perhaps a simulation artifact.